ISSN: 2617-5517 (issn.org)
Al-Farabi Journal of Engineering Sciences
https://iasj.rdd.edu.iq/journals/journal/view/97
مجلة الفارابي للعلوم الهندسية تصدرها جامعة الفارابي

Optimization of machining time and energy consumption through finite element analysis

Author :- Mustafa Fakhri Hamzah
(E-mails: mustafa2421989@gmail.com)

Abstract: Metal cutting is a fundamental industrial process, yet its complexity involving high strain, heating, and diverse operating conditions makes optimization challenging. This study focuses on optimizing two critical parameters in machining: time and energy consumption. Employing the Finite Element Method (FEM) via ANSYS software, the research investigates the intricate mechanics of machining processes. The methodology involved detailed modeling of the problem's geometry, mesh discretization, and convergence analysis to simulate an end mill machining operation. Key findings reveal that tool-workpiece contact points consistently experience maximum stress. Furthermore, an optimal rotational speed between 4000 and 6000 rpm significantly reduces momentum fluctuations and shocks. While kinetic energy increases with rotational speed, reaching a plateau, increasing speeds beyond 8000 rpm yield diminishing returns in energy fluctuation reduction. Importantly, a growing disparity between work done and total energy exchanged at higher speeds indicates increased energy loss. This research provides valuable insights into enhancing machining efficiency and reducing energy waste through FEM analysis, offering practical implications for industrial applications."

Keywords: Finite Element Method (FEM), Machining Optimization, Energy Consumption, Machining Time, ANSYS, Stress Distribution

1. Introduction

Metal cutting, or machining, is a crucial manufacturing operation, essential across multiple industries as it directly or indirectly imparts the final shape and dimensions to nearly all products. This process is intrinsically intricate, marked by significant stresses and heat loads, as well as varied operating circumstances that set it apart from alternative production techniques [1]. The choice of input parameters, including cutting settings, tool geometry, and the material properties of both the workpiece and tool, significantly affects the output factors, with even little modifications possibly resulting in substantial performance variations [2].

Ongoing endeavors are focused on comprehending the complex mechanics of metal cutting using direct and efficient methods. Although conventional trial-and-error approaches are still common in research, a range of scientific models, from basic analytical equations to intricate computer-based numerical simulations, have been established as the foundation of metal cutting theory. In contemporary production, energy-efficient machining is essential for energy conservation. The energy characteristics of machining are intricate and vary significantly with different machine tool configurations, workpieces, and process factors [3]. Moreover, machining procedures substantially influence remanufacturing expenses, component quality, and ecological impact. Thus, optimizing remanufacturing machining pathways presents a significant problem, frequently worsened by the subjective nature of methodologies utilized by previous researchers [4]. This study aims to optimize the critical parameters of time and energy usage in machining processes. Our methodology employs the Finite Element Method (FEM),

specifically leveraging ANSYS software for an extensive examination. Machining involves diverse material removal methods that convert an initial workpiece into a specified final component. The operations are categorized into four main types: turning, drilling, milling, and specialized machining techniques. Although turning, drilling, and milling are prevalent in industry, specialized machining processes encompass advanced techniques such as grinding, sawing, Electrical Discharge Machining (EDM), Electrochemical Machining (ECM), laser cutting, and water jet cutting. The selection of machining technique is determined by particular criteria concerning part geometry, surface finish, and required precision.

Comprehending the fundamental research in this domain is crucial. Multiple research have utilized FEM to examine and enhance different facets of machining. Özell and Altan (2000) devised a finite element method (FEM) system to simulate flat-end milling, forecasting chip flow, cutting forces, tool stresses, and temperatures [5]. Bouzakis et al. (2000) conducted a systematic investigation of the fatigue and wear characteristics of PVD coatings on cemented carbide substrates in milling using FEM simulations [6]. Rao and Shin (2001) performed an analytical and experimental investigation on high-speed milling of T6-7075 aluminum, noting shear localization at elevated feed rates [7]. Debongnie and Beckers (2001) developed a simulation tool to emulate machined surface defects in milling and turning by finite element method (FEM) [8]. Sasahara et al. (2001) employed finite element method (FEM) to examine the temperature of cutting tools in high-speed milling, emphasizing swift temperature fluctuations [9]. Suh et al. (2002) subsequently presented composite designs for machine tool slides to improve damping and save weight [10]. Ratchev et al. (2004) introduced a finite element method (FEM) for simulating material removal that considers part deflection [11]. Mann et al. (2004) employed Time Finite Element Analysis (TFEA) to evaluate accuracy, stability, and force cycle behavior in milling [12]. Wang et al. (2005) utilized the Johnson-Cook model in finite element method (FEM) for milling titanium alloy [13]. Recent studies encompass Guo et al. (2009) on milling distortion analysis for multi-frame components [14], Andoko et al. (2020) who developed a novel cutting force model for side milling [15], and Wang et al. (2021) who proposed a three-dimensional macroscopic milling model for CFRP to predict inter- and intralayer cracking [16]. Chauhan et al. (2022) conducted an extensive review of finite element method (FEM) techniques in amplified milling [17]. Binali et al. (2022) examined power consumption in the milling of AISI P20 steel with finite element method (FEM) [18]. He et al. (2022) executed three-dimensional finite element simulations of milling carbon/epoxy composites [19], whereas Zhou et al. (2023) formulated a three-dimensional finite element model of a side milling cutter in ABAQUS [20].

This study tackles the imperative of optimizing machining processes by concentrating on the reduction of machining time and energy consumption, which are significant issues in contemporary manufacturing. The study methodically examines the end mill machining process via an extensive finite element analysis (FEA) utilizing ANSYS Workbench. A comprehensive methodology was established, including geometry loading, mesh discretization, and convergence analysis, to precisely model the intricate interactions occurring during milling. Principal findings indicate that peak loads are consistently localized at the tool-workpiece interface, and an ideal rotating velocity ranging from 4000 to 6000 rpm substantially reduces momentum variations and related impacts. Although both kinetic and internal energies rise with increased rotational speeds, the research indicates that speeds over 8000 rpm do not produce significant additional reductions in energy fluctuations. Moreover, a significant escalation in the disparity between labor performed and total energy transferred was noted at increased rotational velocities, signifying augmented energy dissipation. These insights offer essential assistance for augmenting machining efficiency, enhancing part quality by alleviating residual stresses, and promoting energy conservation in industrial applications.

.

1. Modeling of the proposed method

In FEM, as the components diminish in size, the constructed thing increasingly approximates reality. This study employs the notion of limit in mathematics, which facilitates the representation or approximation of a uniform object through a finite number of small components; augmenting the quantity of these components enhances the fidelity of the model. The Finite Element Method (FEM) is applicable in resolving mathematical models for numerous engineering challenges, including stress analysis of frame and truss structures, intricate machinery, and the dynamic responses of vehicles such as cars, trains, and airplanes subjected to diverse mechanical, thermal, or electromagnetic loads [21].

In recent decades, numerous commercial programs have emerged for conducting finite element analysis. ANSYS Workbench is an intuitive framework for integrating the ANSYS simulation software suite, among the diverse array of simulation solutions provided by prominent engineering software businesses.

Post-processing: acquiring the necessary quantities, including velocities and pressures. In straightforward scenarios involving systems like springs or trusses, the behavior of the components can be explicitly specified, eliminating the necessity to analyze the governing differential equation. Examine the subsequent differential equation along with its boundary conditions to determine φ(x) for the interval $0 < x < L$.

$$-\frac{d}{dx}\left[a(x)\frac{d\varphi}{dx}\right] = q(x) \qquad (1)$$

$$\varphi(0) = \varphi_0 \,, \left(a\frac{d\varphi}{dx}\right)_{x=L} = Q_0$$

In this context, a and q are defined functions of the x-coordinate, φ_0 and Q_0 are specified values, and L represents the length of the one-dimensional domain. The functions a and q, the constants φ_0 and Q_0, and the domain length constitute the problem's data. φ is the variable that depends on other factors in this situation. Boundary conditions are termed heterogeneous when specific values are non-zero, and homogeneous when particular values are equal to zero ($Q_0 \neq 0$, $\varphi_0 \neq 0$).

Equations of this nature, for instance, arise in the analysis of heat conduction within a heat exchanger fin including an axially symmetric cylinder. The primary objective of formulating the weighted integral expression for the differential equation is to provide a mechanism for deriving n independent linear algebraic relations among the coefficients for the subsequent approximation.

$$\varphi = \sum_{j=1}^{n} c_j \varphi_j + \varphi_0(x) \qquad (2)$$

This can be achieved by selecting n separate linear weight functions in the integral expression provided below. The derivation of the weak form of a differential equation, if applicable, involves three stages. The differential equation and the boundary conditions of the sample delineate these steps.

Initially, all terms of the differential equation are consolidated on one side, after which the weight function w is multiplied by the entire equation and integrated throughout the problem's domain.

$$\int_0^L w\left[-\frac{d}{dx}\left(a\frac{d\varphi}{dx}\right) - q\right]dx = 0 \qquad (3)$$

Step Two: While the weighted integral expression makes it possible to obtain n algebraic relations between C_j's for n arbitrary different weighting functions, it requires the shape (approximation) functions of φ_j to be such that φ is integrable to the number given in the original differential equation.

$$\int_0^L \left\{ w\left[-\frac{d}{dx}\left(a\frac{d\varphi}{dx} \right) \right] - wq \right\} dx = \int_0^L \left(\frac{dw}{dx}\, a\frac{d\varphi}{dx} - wq \right) dx - \left[wa\frac{d\varphi}{dx} \right]_0^L \quad (4)$$

that the relation of integration part by part is given in the following relation.

$$\int_0^L \mathrm{w}.\,\mathrm{d}\varphi = -\int_0^L \varphi.\,dw + [w\varphi]_o^L \quad (5)$$

The crucial aspect of the second phase is to delineate two categories of natural and fundamental boundary conditions pertinent to each differential equation. Upon altering the derivation between the weight function and the variables, specifically after finalizing the second step, all boundary terms of the integral relation are verified. The boundary expressions will encompass both the weight function and the dependent variable. The coefficients of the weight function and its derivatives in the boundary expressions are referred to as secondary variables. The identification of secondary variables at the boundary constitutes the natural boundary conditions. In the current state, the boundary term is wa dφ/dx. The coefficients of the weight function are a dφ/dx. Consequently, the secondary variable is dφ/dx. Secondary variables consistently possess a physical significance. In heat transfer issues, the secondary variable denotes the quantity of heat Q. This variable is articulated as follows:

$$Q = a\left(\frac{d\varphi}{dx}\right) n_x \quad (6)$$

where n_x denotes the cosine of the conductor, equivalent to the cosine of the angle between the x-axis and the direction orthogonal to the boundary. In one-dimensional issues, the direction perpendicular to the boundary points consistently aligns with the length of the domain. Consequently, at the left boundary of the domain, n_x equals -1, while at the right boundary, n_x equals +1.

$$n_x(L) = +1\,, \qquad n_x(0) = -1 \quad (7)$$

The dependent variable, analogous to the weight function in the boundary expression, is referred to as the primary variable, and its value at the boundary establishes the fundamental boundary condition. In the desired state, the dependent function φ serves as the principal variable, and the fundamental boundary condition will specify a particular value of φ at the boundary points. In the given quadratic equation, there exists a principal variable φ and a subordinate variable Q. At the boundary point, only one of the two variables (φ, Q) may be ascertained. In a quadratic equation, such as the classical theory of beams (specifically, Euler-Bernoulli theory), there exist two major variables and two secondary variables. A 2m degree differential equation typically contains m pairs of primary and secondary variables. Equation 7 is represented as follows:

$$\int_0^L \left(a \frac{dw}{dx} \frac{d\varphi}{dx} - wq\right) dx - (wQ)_0 - (wQ)_L = 0 \quad (8)$$

Step Three: The final stage of establishing weak linkages involves implementing the accurate boundary conditions pertinent to the problem under examination. The weight function w at the boundary sites, where the fundamental boundary conditions are established, must equal zero. In other terms, w must comply with the homogeneous version of the specified fundamental boundary conditions of the problem. In the classification of boundary conditions, $\varphi=\varphi_0$ represents the fundamental boundary condition, whereas $(a\, d\varphi/dx)_{(x=L)}=Q$ denotes the normal boundary condition. Consequently, the weight function w must adhere to the subsequent requirements. $w(0) = 0$ thus $\varphi(0) = \varphi_0$. Given that $w(0) = 0$

$$Q(L) = \left(a \frac{d\varphi}{dx} n_x\right)_{x=L} = \left(a \frac{d\varphi}{dx}\right)_{x=L} = Q_0$$

Equation 9 is reduced to the following expression.

$$\int_0^L \left(a \frac{dw}{dx} \frac{d\varphi}{dx} - wq\right) dx - w_{(L)} Q_0 = 0 \quad (9)$$

2. Simulation and Results

The geometry considered for the current research is shown in Figure 1.

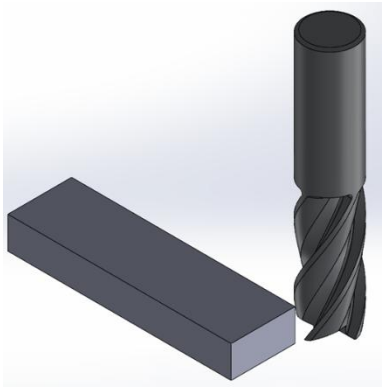

a

b

c

Figure 1: geometry of tools and parts considered in this study; a) Three-dimensional view, b) up view, c) Sideview

The aforementioned figure illustrates a 16 mm diameter titanium end mill engaged with a 10 mm thick aluminum workpiece, with half of the end mill's diameter in contact with the material. The burr removes a thickness of 2 mm from the item. The selection process for the right element begins with the specification of the categories of elements applicable to the current analysis, as determined by the Ansys Fluent software. Subsequent to delineating the categories of items permissible for use Utilize; For each element type with specified boundary conditions, the element size is adjusted, and a key output parameter is documented at each size modification step. Upon analyzing the resultant outputs, it is evident that within a specific range of element dimensions exhibiting little variation in output values, these dimensions are deemed the most appropriate. Figure 2 illustrates the stress distribution contours during machining operations at various time intervals.

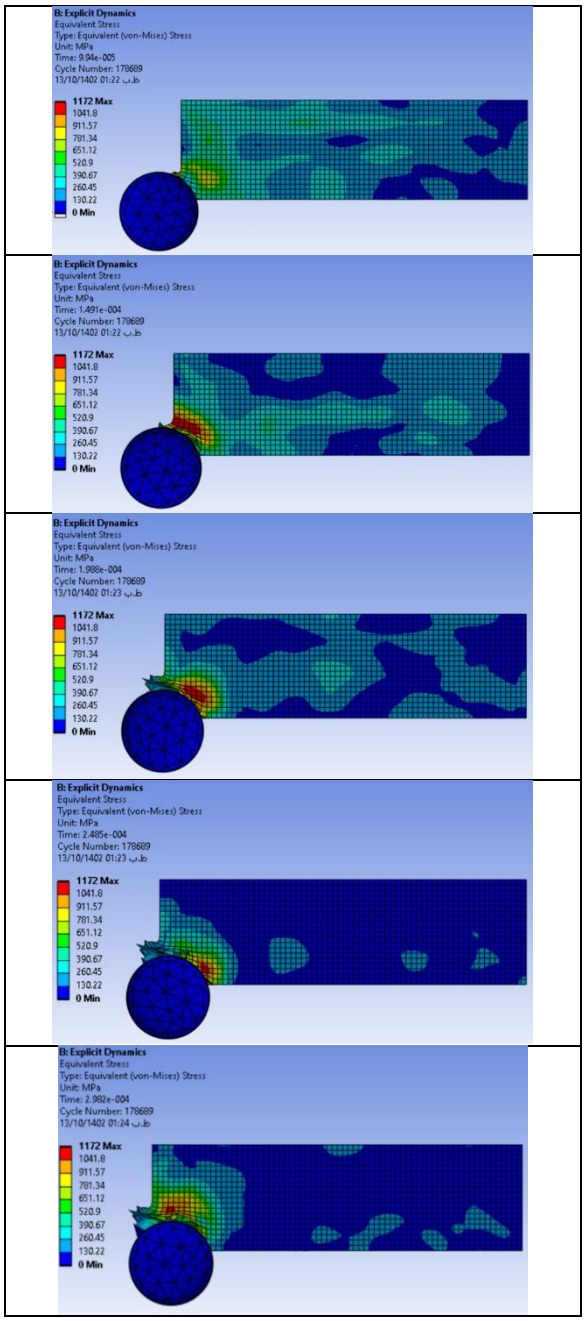

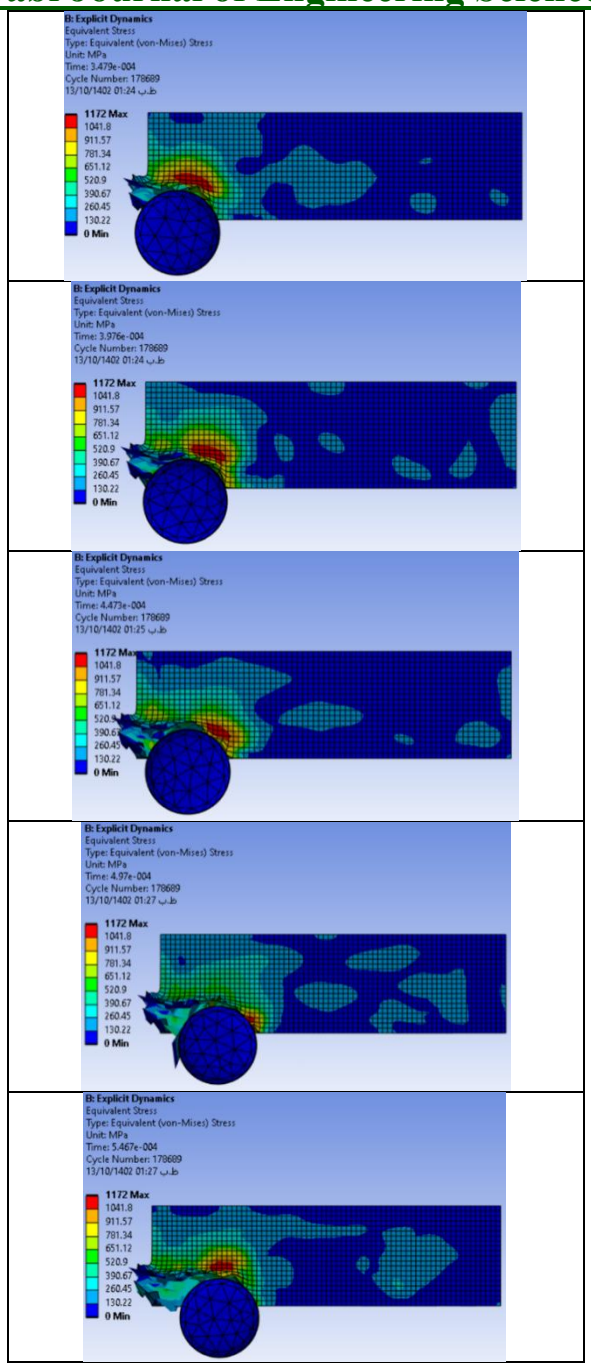

Figure 2: stress distribution contour during machining operation

According to what can be seen in figure 2, the maximum stress created in the part is always created around the contact point of the tool with the work piece. It can also be seen that during the early times of the tool engaging with the part, stresses of about 130 to 260 MPa are created in scattered and wide areas of the part surface, which is because the initial path of the tool on the part is not smooth. It is a part and with the advance of the tool and the formation of the path of the tool movement on the part, this stress distribution is reduced and the stress distribution remains only in the areas adjacent to the machining place. Another point that can be seen in this figure is that after the tool passes through the machined areas, despite the fact that the tool is not involved with those areas, significant amounts of stress remain in these areas. The remaining after the tool passes through the machined areas are the residual stresses created in the piece, which are due to plastic deformation due to cutting of the material in these areas, which after loading (the passage of the tool) through these areas and the return of elastic deformations, still remain in the piece.

Momentum changes during machining time for four speeds of 4000, 6000, 8000 and 10000 rpm are shown in Figure 3. As can be seen in the figure, at a rotational speed of 4000 rpm, the momentum changes along the machining path (x axis) are very high and, as a result, the blows created by these momentum changes are also very high, but with the increase When the speed reaches 6000 rpm, the amount of these fluctuations and shocks is reduced and finally, when the speed reaches 8000 rpm, these shocks reach their minimum value. But by increasing the speed of the tool revolution to 10000 rpm, there are no more specific changes in the behavior of the montum. Therefore, it can be said that the optimal speed for reducing shocks and engine changes is something between 4000 and 6000 rpm.

Among the other points shown in these figures is that the momentum and impact in the direction perpendicular to the machining path (y-axis) fluctuates in the range close to zero, and the reason for that is the rotational collisions of the tool tip with the part, and the momentum values in this Straight enters. But in the direction of the central axis of the tool (z-axis), no change of momentum and no value has been recorded for it, because both the part and the tool are fixed in this direction and the movement constraint is closed for them.

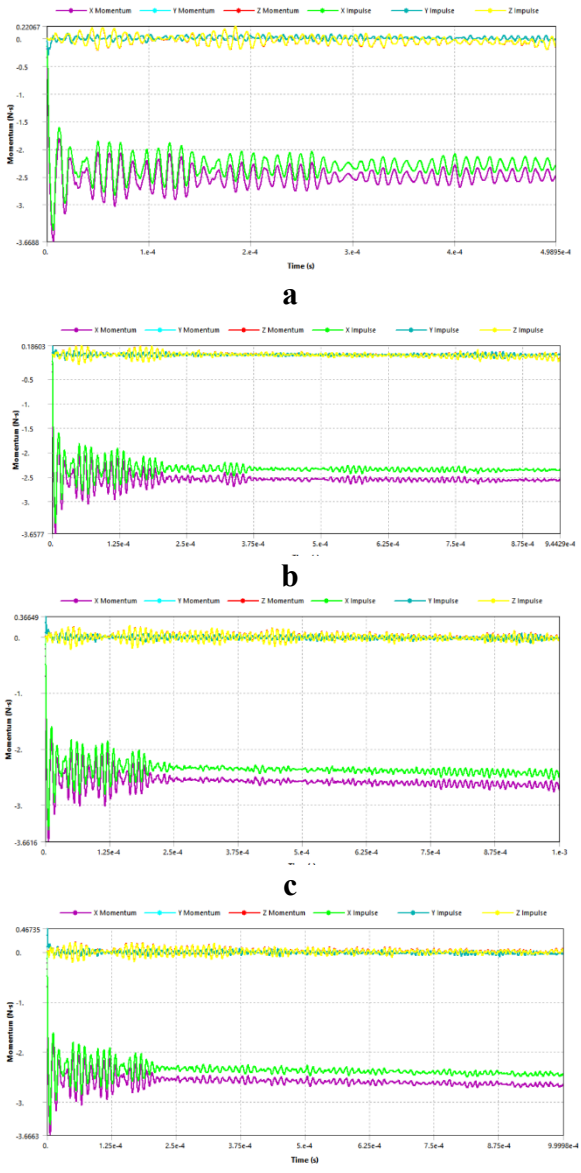

Figure 3: Momentum changes during the machining process; a) 4000 ,b) 6000 , c) 8000 and d) 10000

Figure 4 shows the changes in different forms of energy for the four rotational speeds mentioned. In these figures, it can be seen that the kinetic energy of the assembly increases continuously with the

increase of the rotation speed. So that it reaches from 37500 joules at the rotational speed of 4000 rpm to 22000 joules at the rotational speed of 10000 rpm, but after reaching its maximum value, the amount of this energy remains constant until the end of the machining time, because There is no big change in the movement speed of tools and parts. Also, it can be seen in these figures that the internal energy at all rotational speeds from values close to zero at zero instant reaches higher values with a jump and throughout the machining process, its value is continuous. Increases.

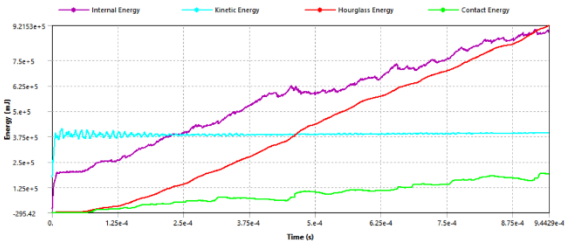

a

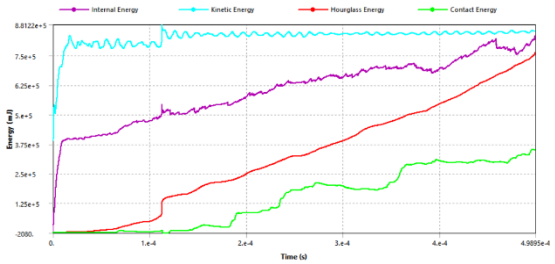

b

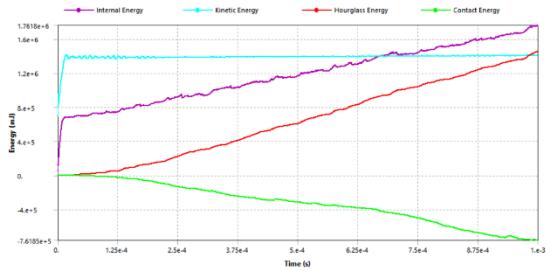

c

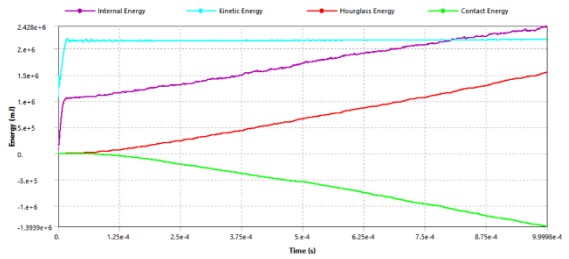

d

Figure 4: Changes in different forms of energy; a) 4000 ,b) 6000 , c) 8000 and d) 10000

Another important point that can be seen in the above figures is the reduction of the fluctuations of different forms of energy during the machining process by increasing the speed of the tool cycle. As can be seen in these diagrams, increasing the speed of the tool rotation causes a sharp reduction in energy fluctuations in the set, but as can be seen in these figures, the decrease in energy fluctuations after the speed of 8000 rpm will not be very significant. The overall changes in energy and work done are shown in Figure 5. In these figures, it can be seen that with the increase of the rotational speed of the tool and with the passage of time, the work done in the machining process increases. But by looking carefully in these graphs, we can see that with the increase in rotation speed, the difference between the work done and the total energy exchanged increases significantly. So that if this difference of work and energy exchanged at the end of the process is drawn with different speeds, the diagram of Figure 6 is drawn.

Carefully in the this figure, it can be seen that with the increase of rotation speed, the slope of the graph of the difference between the work done and the exchanged energy increases increasingly, which is a sign of more and more energy loss.

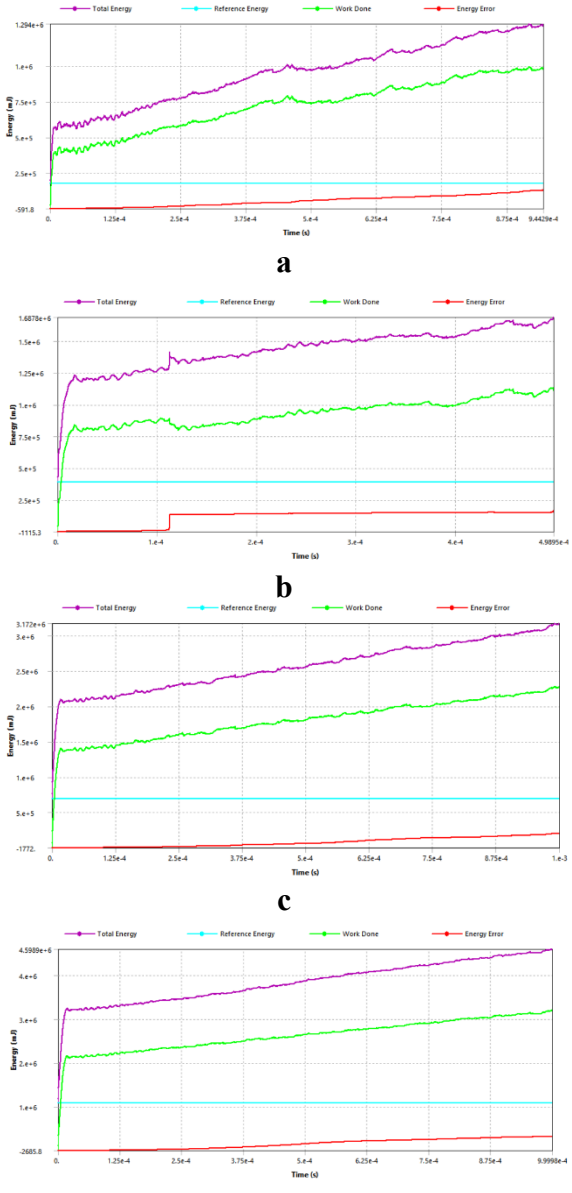

Figure 5: Changes in total energy and work done; a) 4000 ,b) 6000 , c) 8000 and d) 10000

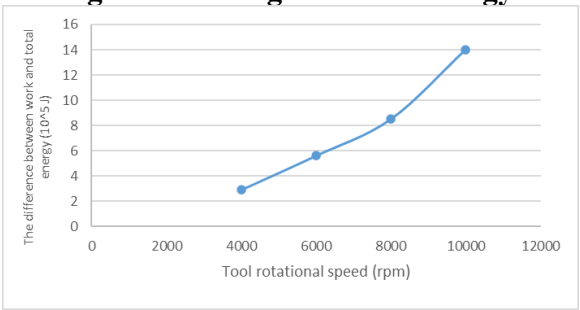

Figure 6: the difference between the work done and the energy exchanged

4. Conclusion

This research successfully utilized the Finite Element Method (FEM) within ANSYS Workbench to simulate and analyze the end mill machining process, specifically focusing on the optimization of machining time and energy

consumption. The study provided critical insights into stress distribution, momentum changes, and energy dynamics under varying rotational speeds. Key findings indicate that maximum stresses consistently occur around the tool-workpiece contact zone. An optimal rotational speed between 4000 and 6000 rpm was identified for significantly minimizing momentum fluctuations and associated shocks. While kinetic and internal energies generally increase with rotational speed, the study revealed that increasing speeds beyond 8000 rpm offers no significant further reduction in energy fluctuations. Crucially, a growing disparity between the work done and total energy exchanged at higher rotational speeds was observed, pointing towards increased energy loss. These results offer valuable guidance for enhancing machining efficiency, improving part quality by mitigating residual stresses, and reducing energy waste in industrial applications. Future work could extend this analysis to explore different tool geometries, workpiece materials, or advanced machining strategies to further refine optimization parameters

References

[1] Cutting, Modern Metal, A. Practical Handbook, and Sandvik Coromant. *Idereklam, Sandviken, Sweden, First North American Edition Edition Pub. 1996, ISBN 91-97 22 99-3-0, pp*. X-45-X-55, 1996.

[2] Akdemir, Ahmet, Şakir Yazman, Hacı Saglam, and Mesut Uyaner. "The effects of cutting speed and depth of cut on machinability characteristics of austempered ductile iron." (2012): 021013.

[3] Zhao, Junhua, Li Li, Lingling Li, Yunfeng Zhang, Jiang Lin, Wei Cai, and John W. Sutherland. "A multi-dimension coupling model for energy-efficiency of a machining process." *Energy* 274 (2023): 127244.

[4] Liu, ChangYi, Xu Meng, Conghu Liu, and Zhi Liu. "Carbon footprint-based optimization method for remanufacturing machining paths." *The International Journal of Advanced Manufacturing Technology* 124, no. 10 (2023): 3391-3406.

[5] Özel, Tuğrul, and Taylan Altan. "Process simulation using finite element method—prediction of cutting forces, tool stresses and temperatures in high-speed flat end milling." International Journal of Machine Tools and Manufacture 40, no. 5 (2000): 713-738.

[6] Bouzakis, K-D., N. Michailidis, N. Vidakis, K. Efstathiou, T. Leyendecker, G. Erkens, R. Wenke, and H-G. Fuss. "Optimization of the cutting edge radius of PVD coated inserts in milling considering film fatigue failure mechanisms." Surface and Coatings Technology 133 (2000): 501-507.

[7] Rao, Balkrishna, and Yung C. Shin. "Analysis on high-speed face-milling of 7075-T6 aluminum using carbide and diamond cutters." International Journal of Machine Tools and Manufacture 41, no. 12 (2001): 1763-1781.

[8] Luc, Jean-François Debongnie, and Pierre Beckers. "Face milling and turning simulation with the finite element method." In The 4th International ESAFORM Conference on Material Forming. ULg-Université de Liège, Liège, Belgium, 2001.

[9] Sasahara, Hiroyuki, Takehiko Nitta, and Kazufumi Nishi. "Analysis of tool temperature in high-speed milling." In Initiatives of Precision Engineering at the Beginning of a Millennium: 10 th International Conference on Precision Engineering (ICPE) July 18–20, 2001, Yokohama, Japan, pp. 279-283. Springer US, 2002.

[10] Suh, J. D., Dai Gil Lee, and R. Kegg. "Composite machine tool structures for high speed milling machines." CIRP Annals 51, no. 1 (2002): 285-288.

[11] Soo, S. L., D. K. Aspinwall, and R. C. Dewes. "Three-dimensional finite element modelling of high-speed milling of Inconel 718." Proceedings of the Institution of Mechanical Engineers, Part B: Journal of Engineering Manufacture 218, no. 11 (2004): 1555-1561.

[12] Ratchev, Svetan, Stan Nikov, and Idir Moualek. "Material removal simulation of peripheral milling of thin wall low-rigidity structures using FEA." Advances in Engineering Software 35, no. 8-9 (2004): 481-491.

[13] Mann, Brian P., Phil V. Bayly, M. A. Davies, and J. E. Halley. "Limit cycles, bifurcations, and accuracy of the milling process." Journal of Sound and Vibration 277, no. 1-2 (2004): 31-48.

[14] Wang, Z. G., M. Rahman, Y. S. Wong, and X. P. Li. "A hybrid cutting force model for high-speed milling of titanium alloys." CIRP annals 54, no. 1 (2005): 71-74.

[15] Guo, H., D. W. Zuo, H. B. Wu, F. Xu, and G. Q. Tong. "Prediction on milling distortion for aero-multi-frame parts." Materials Science and Engineering: A 499, no. 1-2 (2009): 230-233.

[16] Andoko, Andoko, Retno Wulandari, Dhanang Reza Pradica, Pradhana Kurniawan, Raymond Philander Jeadi, Riduwan Prasetya, Agus Dwi Putra, and Galih Adhi Kurniawan. "Simulation on CNC 5 axis milling spindle bolt using finite element method." In AIP Conference Proceedings, vol. 2262, no. 1. AIP Publishing, 2020.

[17] Wang, Fuji, Tianyu Gu, Xiaonan Wang, Xinghai Jin, and Boyu Zhang. "Analysis of burr and tear in milling of carbon fiber reinforced plastic (CFRP) using finite element method." Applied Composite Materials 28, no. 4 (2021): 991-1018.

[18] Chauhan, Shailendra, Rajeev Trehan, and Ravi Pratap Singh. "State of the art in finite element approaches for milling process: a review." Advances in Manufacturing (2022): 1-44.

[19] Binali, Rüstem, Mücahit Coşkun, and Süleyman Neşeli. "An investigation of power consumption in milling AISI P20 plastic mold steel by finite elements method." Avrupa Bilim ve Teknoloji Dergisi 34 (2022): 513-518.

[20] He, Yanli, Long Li, Min Wan, and Hongqian Xue. "Three-dimensional finite element simulations of milling carbon/epoxy composites." Composite Structures 282 (2022): 115037.

[21] Zhu, Xiaohua, Jiangmiao Shi, and Yunhai Liu. "Effect of Declination Angle on the Side Milling Process of Ti6Al4V by a New Three-Dimensional Milling Finite Element Model." Journal of Materials Engineering and Performance (2023): 1-10.